ACS PHYSICAL CHEMISTRY Au
AN OPEN ACCESS JOURNAL OF THE AMERICAN CHEMICAL SOCIETY

Open Access
This article is licensed under CC-BY-NC-ND 4.0

pubs.acs.org/physchemau
Letter

Molecular CO_2 Storage: State of a Single-Molecule Gas

Yoshifumi Hashikawa,* Shumpei Sadai, and Yasujiro Murata*

Cite This: ACS Phys. Chem Au 2024, 4, 143–147
Read Online
ACCESS | Metrics & More | Article Recommendations | Supporting Information

ABSTRACT: CO_2 evolution is one of the urgent global issues; meanwhile, understanding of sorptive/dynamic behavior is crucial to create next-generation encapsulant materials with stable sorbent processes. Herein, we showcase molecular CO_2 storage constructed by a [60]fullerenol nanopocket. The CO_2 density reaches 2.401 g/cm^3 within the nanopore, showing strong intramolecular interactions, which induce nanoconfinement effects such as forbidden translation, restricted rotation, and perturbed vibration of CO_2. We also disclosed an equation of state for a molecular CO_2 gas, revealing a very low pressure of 3.14 rPa (1 rPa = 10^{-27} Pa) generated by the rotation/vibration at 300 K. Curiously enough, the CO_2 capture enabled to modulate an external property of the encapulant material itself, i.e., association of the [60]fullerenol via intercage hydrogen-bonding.

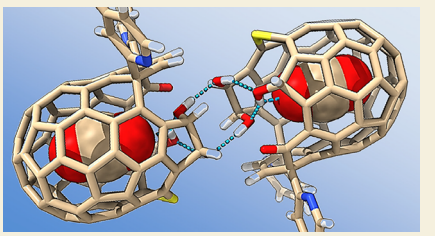

KEYWORDS: *carbon dioxide, nanocarbon, single molecule, supramolecular assembly, open-[60]fullerene*

Solid sorbent systems for CO_2 capture/storage have been recognized as viable generators of a recyclable carbon source to tackle the global issue that plenty of CO_2 has been continuously emitted and accumulated in the course of industrial and biological processes.[1] As solid sorbents, porous materials such as zeolite,[2] mesoporous silica,[3] and metal–organic frameworks (MOFs)[4] have been developed in materials science, targeting efficient/selective capture and facile release of CO_2 with a low energy cost. Within the sorbents, CO_2 is captured by chemisorption and/or physisorption where CO_2 is converted into carbamate species by a surface-functionalized interior for the former, while, in the latter case, it binds to Lewis acidic/basic sites such as metal centers and/or active ligands via weak intermolecular interactions.[5]

High polarizability and quadrupolar characteristics of CO_2, however, cause a labyrinth of a physical picture on sorptive/dynamic behavior through a mixed interplay of dispersion forces and electrostatic interactions.[6] In addition, at higher CO_2 coverages, it undergoes dimerization and/or a change in coordinates from linear to bent within pores.[7] These multiple factors interfere with each other, thus severely reducing opportunities to gain definitive mechanistic insights into chemisorption/physisorption as well as the physical nature of the confined CO_2 gas, both of which have been poorly understood on a molecular scale.[8] Hence, molecular CO_2 storage that could experimentally model simple interior sorption is highly demanded for further designing pore functionalities of encapsulant materials. Herein, we focus on open-[60]fullerenols[9] (Figure 1), which are suitable for exploiting the nanoconfinement effect of captured species such as the acid/base character of gaseous H_2O[10] and paramagnetism of NO.[11] In this paper, we examined the sorptive/dynamic behavior and equation of state for a single molecule of CO_2 gas as well as the nanoconfinement effect on its vibrational behavior. We also discuss a remote property modulation of the [60]fullerene container, which is caused by the internal CO_2 molecule.

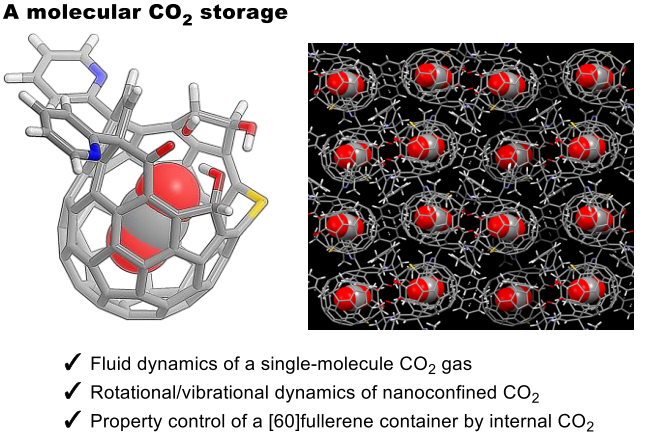

Figure 1. [60]fullerene-based molecular CO_2 storage.

Precursor host **1** contains water, nitrogen, and argon owing to a spontaneous encapsulation.[12] To gain a reasonable occupancy of CO_2 by emitting the precaptured species, CO_2 insertion was performed in *o*-dichlorobenzene (ODCB) at 130 °C under 9000 atm (Figure 2a), while CO_2 could pass through

Received: December 7, 2023
Revised: December 12, 2023
Accepted: December 12, 2023
Published: January 16, 2024

© 2024 The Authors. Published by American Chemical Society

https://doi.org/10.1021/acsphyschemau.3c00068
ACS Phys. Chem Au 2024, 4, 143–147

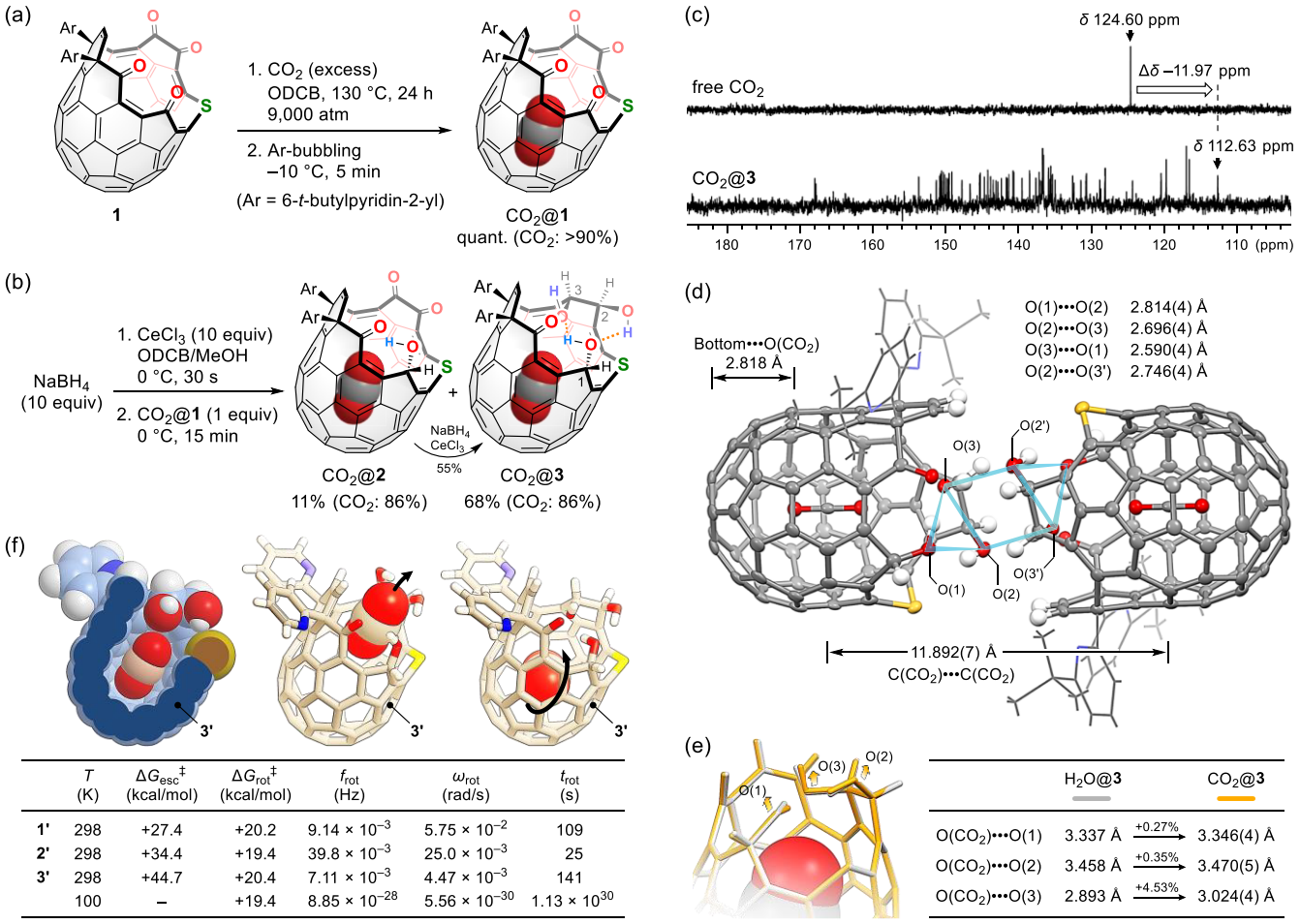

	T (K)	$\Delta G_{esc}^{\ddagger}$ (kcal/mol)	$\Delta G_{rot}^{\ddagger}$ (kcal/mol)	f_{rot} (Hz)	ω_{rot} (rad/s)	t_{rot} (s)
1'	298	+27.4	+20.2	9.14×10^{-3}	5.75×10^{-2}	109
2'	298	+34.4	+19.4	39.8×10^{-3}	25.0×10^{-3}	25
3'	298	+44.7	+20.4	7.11×10^{-3}	4.47×10^{-3}	141
	100	–	+19.4	8.85×10^{-28}	5.56×10^{-30}	1.13×10^{30}

Figure 2. (a) Placing gaseous CO_2 inside **1**. (b) Synthesis of molecular CO_2 storage. (c) ^{13}C NMR spectra (500 MHz, $CDCl_3/CS_2$ (1:1)) of free CO_2 and CO_2@**3**. (d) Crystal structure of $(CO_2@\mathbf{3})_2$ showing thermal ellipsoids at 50% probability (solvent molecules are omitted for clarity). (e) Overlay of crystal structures for H_2O@**3** and CO_2@**3** with selected bond lengths. (f) Thermodynamic parameters on CO_2 inside **1′**, **2′**, and **3′** (Ar = 2-pyridyl; B3LYP-D3/6-31G(d); $\Delta G^{\ddagger}$, barriers for escape/rotation; f_{rot}, rotational frequency; ω_{rot}, angular velocity; t_{rot}, time required for a full turn of 2π radians).

the orifice even under ambient conditions. The occupancy was determined to be >90% from a signal splitting of the addends by ^1H NMR. After removing CO_2 dissolved in ODCB by Ar bubbling at −10 °C, the Luche reduction was applied to afford CO_2@**2**[13] and CO_2@**3** (Figure 2b). The occupancy for CO_2@**3** was enriched to be 100% from 86% by recycle HPLC. The presence of captured CO_2 was confirmed by ^{13}C NMR (500 MHz, $CDCl_3/CS_2$ (1:1)) showing its signal at δ 112.63 ppm, which was higher-field shielded, by $\Delta\delta$ −11.97 ppm, from free CO_2 (δ 124.60 ppm), owing to the [60]fullerene aromaticity[14] (Figure 2c). The X-ray diffraction (XRD) analysis at 100 K revealed a dimeric configuration of CO_2@**3** structured by multiple hydrogen bondings arranged in a chair-like shape (Figure 2d), being reminiscent of fullertubes.[15] Within the crystal, the two CO_2 molecules are precisely separated with a distance of 11.892(7) Å on a shared axis. Captured CO_2 most likely interacts with the [60]fullerenol upon seeing close contacts with the carbon wall. The amount of adsorbed CO_2 in crystal (Figure 1) was estimated to be 0.247 cm^3/cm^3 (1 atm, 25 °C), which is smaller than those for MOFs (90−200 cm^3/cm^3).[16] However, the CO_2 density in nanopore (ρ) is as large as 2.401 g/cm^3, which exceeds the highest value reported among MOFs (0.955 g/cm^3)[16] and is 2-fold larger than that of liquid CO_2 (1.178 g/cm^3 at the triple point[17]), indicating a dense packing of molecular CO_2 within the nanocavity. The crowded arrangement of the three hydroxy groups renders a pore volume (V = 30.4 $Å^3$) smaller by −8.9% than **1** (33.4 $Å^3$),[12] which contributes to the dense confinement. Figure 2e illustrates a structural overlay of H_2O@**3**[10] and CO_2@**3** obtained by XRD, unveiling the steric repulsion, which results in an extrusion of the three hydroxy groups toward the outside, by up to +4.53%, with a central focus on the oxygen atom in CO_2.

Since a release barrier of CO_2 from **3′** (Ar = 2-pyridyl) was computed to be $\Delta G^{\ddagger}$ + 44.7 kcal/mol at 298 K, **3** could be regarded as permanent CO_2 storage, while CO_2 escape is probable for **1′** (Figure 2f). Within the nanopore, CO_2 rotates with an activation barrier of $\Delta G^{\ddagger}$ + 20.2 kcal/mol, suggestive of a very slow rotation with rotational frequency f_{rot} (7.11 mHz) and time t_{rot} (141 s). At 100 K, a full turn requires 1.13×10^{-30} s so that the rotation of CO_2 is forbidden under the XRD conditions.

Release rates k of CO_2@**1** were measured in $CDCl_3$ by ^1H NMR (Figure 3a), affording thermodynamic parameters: $\Delta G^{\ddagger}$ + 25.1 ± 1.0 kcal/mol, $\Delta H^{\ddagger}$ 22.5 ± 0.7 kcal/mol, and $\Delta S^{\ddagger}$ −8.96 ± 2.24 cal/(K·mol). Upon assuming the release event being ideal fluid dynamics on an atmospheric relief of a

https://doi.org/10.1021/acsphyschemau.3c00068
ACS Phys. Chem Au 2024, 4, 143−147

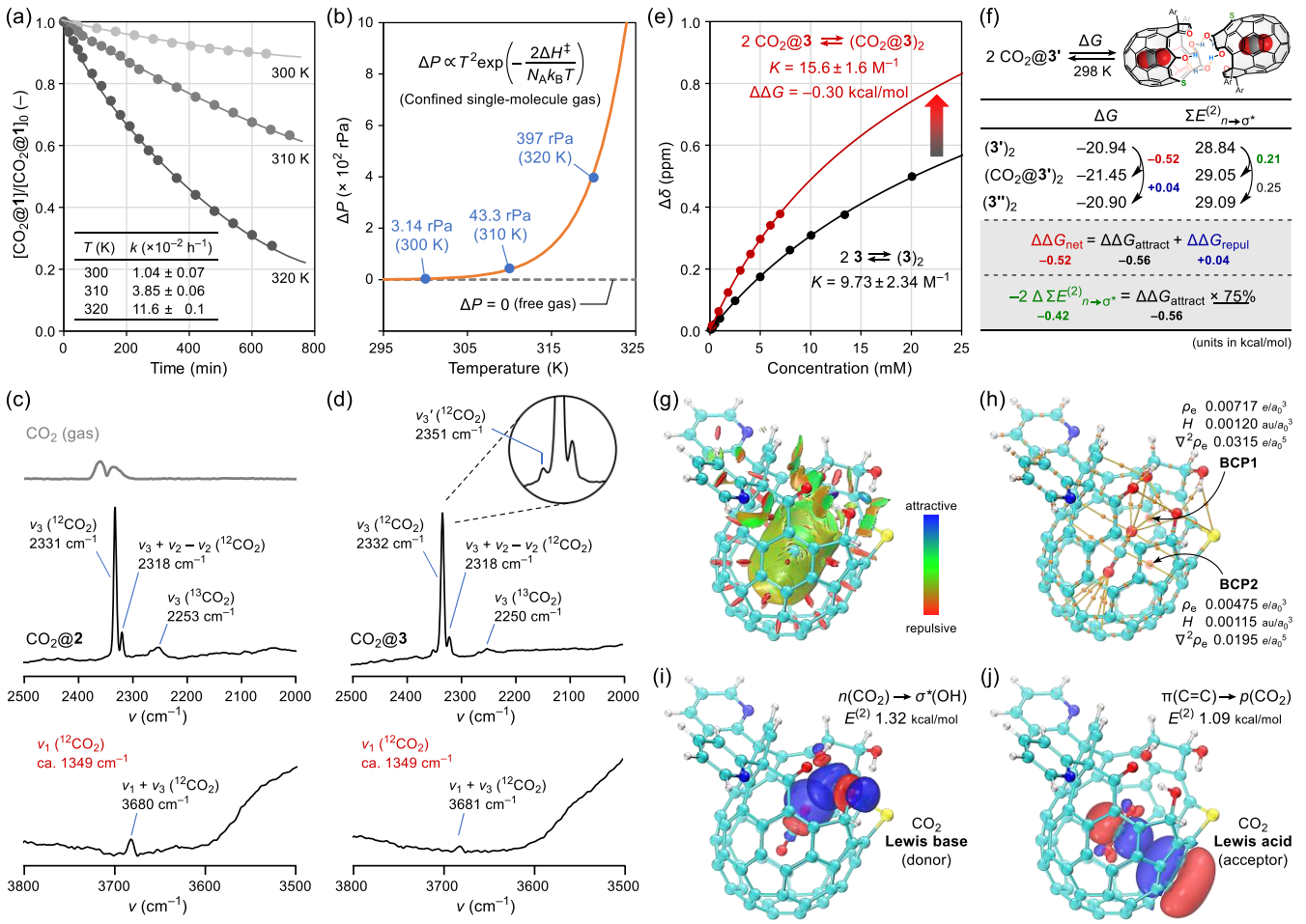

Figure 3. (a) Release rates of CO_2 from **1** in $CDCl_3$. (b) $P-T$ curve of a single molecule of CO_2 gas in **1**. (c,d) IR spectra of free CO_2, CO_2@**2**, and CO_2@**3** (300 K). (e) Binding constants K with stabilization energy $\Delta\Delta G$ induced by CO_2 in **3**, determined by ^1H NMR (500 MHz, $CDCl_3$, 300 K). (f) Calculated stabilization energies ΔG upon dimerization with interaction energies $\Sigma E^{(2)}$ of intermolecular hydrogen-bonding (B3LYP-D3/6-31G(d,p)). **3″** is a distorted empty cage whose coordinates originate from CO_2@**3′**. (g) NCI map of CO_2@**3′**. (h) BCPs and BPs with selected density values. (i,j) NBOs and interaction energies for CO_2@**3′**. All calculations were conducted at B3LYP-D3/6-31G(d,p).

nanoscale vessel containing a CO_2 gas, we applied Bernoulli's equation to describe the conservation of momenta:

$$P_1 = P_2 + \frac{\rho {v_2}^2}{2}$$

where P is static pressure and v is velocity. Note that the second term, i.e., dynamic pressure, is zero at the initial state due to $v_1 = 0$. The density of CO_2 is defined by $\rho = M/(N_A V)$ where M is molecular weight of CO_2 and N_A is Avogadro's constant. The time required for releasing a half quantity of a molecular CO_2 gas (equal to $0.5V$) is then expressed by

$$t_{1/2} = \frac{0.5V}{Av_2} = \frac{V}{2A}\sqrt{\frac{M}{2N_A V(P_1 - P_2)}}$$

where A is the orifice area (4.09 Å^2). Given that the physical event obeys a first-order reaction characterized by $t_{1/2}$, which is measurable by a kinetic study on an ensemble of CO_2@**1** (Figure 3a), the transition state theory gives $t_{1/2}$ as a function of temperature T:

$$t_{1/2} = \frac{\ln 2}{k} = \frac{h\ln 2}{k_B T}\exp\left(\frac{\Delta H^{\ddagger} - T\Delta S^{\ddagger}}{N_A k_B T}\right)$$

where h and k_B are Planck and Boltzmann constants, respectively. Since the dynamic pressure at the final state corresponds to the loss of pressure ($\Delta P = P_1 - P_2$), ΔP is consequently associated with a function of T:

$$\Delta P = CT^2\exp\left(-\frac{2\Delta H^{\ddagger}}{N_A k_B T}\right)$$

$$C = \frac{MV}{8N_A}\cdot\left(\frac{k_B}{Ah\ln 2}\right)^2\exp\left(\frac{2\Delta S^{\ddagger}}{N_A k_B}\right)$$

This is regarded as an equation of state for a single-molecule gas captured within the nanocavity. Figure 3b shows a $P-T$ curve of a single molecule of CO_2 gas. The dynamic pressure at 300 K was estimated to be $\Delta P = 3.14$ rPa (1 rPa = 10^{-27} Pa), which is far smaller than $P_1 = 102$ hPa. Even at 1000 K, it reaches only 3.00 mPa. This is because of a molecular vibration/rotation as a major contributor to the dynamic pressure, while the translational motion is exhaustively forbidden within the cavity. According to the equation, even under $dT = dV = 0$, the gaseous molecule attains an eigen pressure loss. This is in stark contrast to an ensemble whose equation of state ($PV = k_B T$, $\Delta P = 0$ under constant T and V)

https://doi.org/10.1021/acsphyschemau.3c00068
ACS Phys. Chem Au 2024, 4, 143−147

is derived from kinetic theory of gases, solely depending upon translational motion.

To further study rotational/vibrational dynamics of the confined CO_2 gas, we measured IR spectra at 300 K (Figure 3c,d). Linear triatomic CO_2 with a $D_{\infty h}$ symmetry has four fundamental modes of vibration including symmetric and antisymmetric stretching (ν_1 and ν_3) as well as doubly degenerated bending (ν_2), where only ν_2 and ν_3 are IR active. Whereas a band overlap in a fingerprint region was unable to discriminate ν_2 from others originating from skeletal vibration of the carbon cage, $\nu_3(^{12}CO_2)$ was found at 2331 cm^{-1} for CO_2@**2** and 2332 cm^{-1} for CO_2@**3** as a sharp band, which differs from atmospheric CO_2 showing a broad band (2349 cm^{-1})[6] caused by a vibration/rotation coupling (Figure 3c). Within the nanocavity, however, the rotational frequency of CO_2 (10^{-3}–10^{-2} Hz, Figure 2f) is rather larger than the time scale of molecular vibration (10 fs–1 ps),[18] which significantly relaxes the coupling. The observed red-shift of $\Delta\nu_3$ −17 to −18 cm^{-1} relative to free CO_2 is comparable to those observed for CO_2 in typical MOFs (ν_3 2335 cm^{-1}),[7b] implying the presence of interactions to a similar extent. The two bands at lower wavenumbers correspond to a hot band ($\nu_3 + \nu_2 - \nu_2$) and satellite ($\nu_3(^{13}CO_2)$).[19] At a higher wavenumber, CO_2@**3** showed a small band (ν_3' 2351 cm^{-1}), which is unlikely to be found for CO_2@**2**. A metastable orientation of the three hydroxy groups in CO_2@**3** would be a possible explanation, as supported by computational studies (Figure S12). Importantly, a combination band ($\nu_1 + \nu_3$) was observed at 3680 cm^{-1} for CO_2@**2** and 3681 cm^{-1} for CO_2@**3**. From the combination tone, ν_1 was estimated to be ca. 1349 cm^{-1}, which is red-shifted by $\Delta\nu_1$ ca. −39 cm^{-1} relative to free CO_2 (ν_1 1388 cm^{-1}).[6] Though Fermi resonance might not be neglected, this value is as large as 2-fold $\Delta\nu_3$, being suggestive of a strong nanoconfinement effect on the symmetric stretching (ν_1), which offers a larger vibrational displacement than that of the antisymmetric one (ν_3).

To our surprise, the captured CO_2 gas enabled to modulate an external property of the encapulant material itself. The association constant of CO_2@**3** in $CDCl_3$ at 300 K was measured to be K = 15.6 ± 1.6 M^{-1}, which is 1.6-fold larger than that of empty **3** (9.73 ± 2.34 M^{-1}) (Figure 3e). This is suggestive of the preferred association for the latter by $\Delta\Delta G$ −0.30 kcal/mol, being in good accordance with the calculated value of $\Delta\Delta G_{net}$ −0.52 kcal/mol (Figure 3f), which includes attractive (−0.56 kcal/mol) and repulsive (+0.04 kcal/mol) interactions mainly caused by better hydrogen-bonding ($-2\Delta\Sigma E^{(2)}$ −0.42 kcal/mol) and geometrical distortion upon CO_2 capture (Figure 2e), respectively.

A reduced density gradient (RDG) isosurface[20] was plotted for CO_2@**3**′ (Figure 3g), showing weak noncovalent interactions (NCI), around the CO_2 molecule, which were characterized by multiple bond critical points (BCPs) and bond paths (BPs) (Figure 3h).[21] A positive Laplacian of electron density $\nabla^2\rho_e$ and total electron energy density H at BCP1 and BCP2 imply pure closed-shell interactions without a covalent nature. Natural bond orbital (NBO) analysis showed interaction energies as large as $E^{(2)}$ 1.32 ($n(CO_2) \rightarrow \sigma^*(OH)$) and 1.09 ($\pi(C{=}C) \rightarrow p(CO_2)$) kcal/mol, respectively (Figure 3i,j). These results are decisive of the confined CO_2 molecule potentially acting as both a Lewis base and Lewis acid.

In conclusion, we designed molecular CO_2 storage as the simplest experimental model for revealing clear physical pictures on the chemical/dynamic processes of a molecular CO_2 gas confined within a nanoscale cavity, which are otherwise uncertain in known sorbent systems due to competing complex interactions. The combined analyses of XRD, IR, and computations demonstrated the presence of intramolecular interactions in CO_2@**3**, which cause nano-confinement effects on translational, vibrational, and rotational motions of captured CO_2, where it acts as both a Lewis base and Lewis acid. The release event for CO_2@**1** revealed the equation of state for a single-molecule gas at imperceptible pressure levels. The captured CO_2 gas modulated an external property of the encapulant material itself owing to the better arrangement of intermolecular hydrogen-bonding. These findings would facilitate further understandings of chemical/physical events of CO_2 accommodated within a variety of sorbent materials.

■ ASSOCIATED CONTENT

Supporting Information

The Supporting Information is available free of charge at https://pubs.acs.org/doi/10.1021/acsphyschemau.3c00068.

Detailed experimental procedures, characterization data, and computational results (PDF)

Crystallographic data (CIF)

Accession Codes

CCDC 2301301 contains the supplementary crystallographic data for this paper. These data can be obtained free of charge via www.ccdc.cam.ac.uk/data_request/cif, or by emailing data_request@ccdc.cam.ac.uk, or by contacting The Cambridge Crystallographic Data Centre, 12 Union Road, Cambridge CB2 1EZ, UK; fax: + 44 1223 336033.

■ AUTHOR INFORMATION

Corresponding Authors

Yoshifumi Hashikawa − *Institute for Chemical Research, Kyoto University, Uji, Kyoto 611-0011, Japan*; orcid.org/0000-0001-7834-9593; Email: hashi@scl.kyoto-u.ac.jp

Yasujiro Murata − *Institute for Chemical Research, Kyoto University, Uji, Kyoto 611-0011, Japan*; orcid.org/0000-0003-0287-0299; Email: yasujiro@scl.kyoto-u.ac.jp

Author

Shumpei Sadai − *Institute for Chemical Research, Kyoto University, Uji, Kyoto 611-0011, Japan*

Complete contact information is available at: https://pubs.acs.org/10.1021/acsphyschemau.3c00068

Notes

The authors declare no competing financial interest.

■ ACKNOWLEDGMENTS

Financial support was partially provided by the JSPS KAKENHI Grant Number JP23H01784 and JP22H04538, The Mazda Foundation, and Advanced Technology Institute Research Grants 2023. IR measurements were carried out at SPring-8 (BL43IR) with the approval of JASRI (2022B1138). We thank Dr. Yuka Ikemoto for the support on IR spectroscopy.

REFERENCES

(1) Dziejarski, B.; Serafin, J.; Andersson, K.; Krzyżyńska, R. CO_2 capture materials: a review of current trends and future challenges. *Mater. Today Sustain.* **2023**, *24*, 100483.

(2) Boer, D. G.; Langerak, J.; Pescarmona, P. P. Zeolites as Selective Adsorbents for CO_2 Separation. *ACS Appl. Energy Mater.* **2023**, *6*, 2634−2656.

(3) Chen, C.; Zhang, S.; Row, K. H.; Ahn, W.-S. Amine-silica composites for CO_2 capture: A short review. *J. Energy Chem.* **2017**, *26*, 868−880.

(4) Sumida, K.; Rogow, D. L.; Mason, J. A.; McDonald, T. M.; Bloch, E. D.; Herm, Z. R.; Bae, T.-H.; Long, J. R. Carbon Dioxide Capture in Metal-Organic Frameworks. *Chem. Rev.* **2012**, *112*, 724−781.

(5) Vaidhyanathan, R.; Iremonger, S. S.; Shimizu, G. K. H.; Boyd, P. G.; Alavi, S.; Woo, T. K. Direct Observation and Quantification of CO_2 Binding Within an Amine-Functionalized Nanoporous Solid. *Science* **2010**, *330*, 650−653.

(6) Vitillo, J. G.; Savonnet, M.; Ricchiardi, G.; Bordiga, S. Tailoring Metal-Organic Frameworks for CO_2 Capture: The Amino Effect. *ChemSusChem* **2011**, *4*, 1281−1290.

(7) (a) Bonelli, B.; Civalleri, B.; Fubini, B.; Ugliengo, P.; Areán, C. O.; Garrone, E. Experimental and Quantum Chemical Studies on the Adsorption of Carbon Dioxide on Alkali-Metal-Exchanged ZSM-5 Zeolites. *J. Phys. Chem. B* **2000**, *104*, 10978−10988. (b) Mihaylov, M.; Chakarova, K.; Andonova, S.; Drenchev, N.; Ivanova, E.; Sabetghadam, A.; Seoane, B.; Gascon, J.; Kapteijn, F.; Hadjiivanov, K. Adsorption Forms of CO_2 on MIL-53(Al) and NH2-MIL-53(Al) As Revealed by FTIR Spectroscopy. *J. Phys. Chem. C* **2016**, *120*, 23584−23595.

(8) (a) Roztocki, K.; Rauche, M.; Bon, V.; Kaskel, S.; Brunner, E.; Matoga, D. Combining In Situ Techniques (XRD, IR, and ^{13}C NMR) and Gas Adsorption Measurements Reveals CO_2-Induced Structural Transitions and High CO_2/CH_4 Selectivity for a Flexible Metal-Organic Framework JUK-8. *ACS Appl. Mater. Interfaces* **2021**, *13*, 28503−28513. (b) Stolte, N.; Hou, R.; Pan, D. Nanoconfinement facilitates reactions of carbon dioxide in supercritical water. *Nat. Commun.* **2022**, *13*, 5932.

(9) (a) Vougioukalakis, G. C.; Roubelakis, M. M.; Orfanopoulos, M. Open-Cage Fullerenes: towards the Construction of Nanosized Molecular Containers. *Chem. Soc. Rev.* **2010**, *39*, 817−844. (b) Gao, R.; Liu, Z.; Liu, Z.; Liang, T.; Su, J.; Gan, L. Open-Cage Fullerene as a Selective Molecular Trap for LiF/$[BeF]^+$. *Angew. Chem., Int. Ed.* **2023**, *62*, No. e202300151. (c) Hashikawa, Y.; Murata, Y. Water in Fullerenes. *Bull. Chem. Soc. Jpn.* **2023**, *96*, 943−967.

(10) Hashikawa, Y.; Hasegawa, S.; Murata, Y. A Single *but* Hydrogen-Bonded Water Molecule Confined in an Anisotropic Subnanospace. *Chem. Commun.* **2018**, *54*, 13686−13689.

(11) Hashikawa, Y.; Hasegawa, S.; Murata, Y. Precise Fixation of an NO molecule inside Carbon Nanopores: A Long-Range Electron-Nuclear Interaction. *Angew. Chem., Int. Ed.* **2021**, *60*, 2866−2870.

(12) (a) Futagoishi, T.; Murata, M.; Wakamiya, A.; Sasamori, T.; Murata, Y. Expansion of Orifices of Open C_{60} Derivatives and Formation of an Open $C_{59}S$ Derivative by Reaction with Sulfur. *Org. Lett.* **2013**, *15*, 2750−2753. (b) Hashikawa, Y.; Fujikawa, N.; Okamoto, S.; Murata, Y. Phosphorus ylides of cage-opened sulphide [60]fullerene derivatives. *Dalton Trans.* **2022**, *51*, 17804−17808.

(13) Futagoishi, T.; Murata, M.; Wakamiya, A.; Murata, Y. Trapping N_2 and CO_2 on the Sub-Nano Scale in the Confined Internal Spaces of Open-Cage C_{60} Derivatives: Isolation and Structural Characterization of the Host-Guest Complexes. *Angew. Chem., Int. Ed.* **2015**, *54*, 14791−14794.

(14) Taylor, R. Aromatic fullerene derivatives. *Phys. Chem. Chem. Phys.* **2004**, *6*, 328−331.

(15) Koenig, R. M.; Tian, H.-R.; Seeler, T. L.; Tepper, K. R.; Franklin, H. M.; Chen, Z.-C.; Xie, S.-Y.; Stevenson, S. Fullertubes: Cylindrical Carbon with Half-Fullerene End-Caps and Tubular Graphene Belts, Their Chemical Enrichment, Crystallography of Pristine C_{90}-$D_{5h}(1)$ and C_{100}-$D_{5d}(1)$ Fullertubes, and Isolation of C_{108}, C_{120}, C_{132}, and C_{156} Cages of Unknown Structures. *J. Am. Chem. Soc.* **2020**, *142*, 15614−15623.

(16) Ye, Y.; Xiong, S.; Wu, X.; Zhang, L.; Li, Z.; Wang, L.; Ma, X.; Chen, Q.-H.; Zhang, Z.; Xiang, S. Microporous Metal-Organic Framework Stabilized by Balanced Multiple Host-Couteranion Hydrogen-Bonding Interactions for High-Density CO_2 Capture at Ambient Conditions. *Inorg. Chem.* **2016**, *55*, 292−299.

(17) Li, M.; Wang, G.; Sun, L.; Cao, X.; Ni, H. A Possible Explicit Equation Fitting Method for the Gaseous Heat Capacity Near the Critical Point Based on Density and Temperature. *Processes* **2023**, *11*, 1605.

(18) Zewail, A. H. Femtochemistry. Past, present, and future. *Pure Appl. Chem.* **2000**, *72*, 2219−2231.

(19) (a) Meredith, J. C.; Johnston, K. P.; Seminario, J. M.; Kazarian, S. G.; Eckert, C. A. Quantitative Equilibrium Constants between CO_2 and Lewis Bases from FTIR Spectroscopy. *J. Phys. Chem.* **1996**, *100*, 10837−1084. (b) Kim, D.; Park, J.; Kim, Y. S.; Lah, M. S. Temperature dependent CO_2 behavior in microporous 1-D channels of a metal-organic framework with multiple interaction sites. *Sci. Rep.* **2017**, *7*, 41447. (c) Chakarova, K.; Mihaylov, M.; Hadjiivanov, K. Can two CO_2 molecules be simultaneously bound to one Na^+ site in NaY zeolite? A detailed FTIR investigation. *Micro. Meso. Mater.* **2022**, *345*, 112270.

(20) Johnson, E. R.; Keinan, S.; Mori-Sánchez, P.; Contreras-García, J.; Cohen, A. J.; Yang, W. Revealing noncovalent interactions. *J. Am. Chem. Soc.* **2010**, *132*, 6498−6506.

(21) (a) Nakanishi, W.; Hayashi, S.; Narahara, K. Polar Coordinate Representation of $H_b(r_c)$ versus $(\hbar^2/8m)\nabla^2\rho_b(r_c)$ at BCP in AIM Analysis: Classification and Evaluation of Weak to Strong Interactions. *J. Phys. Chem. A* **2009**, *113*, 10050−10057. (b) Hashikawa, Y.; Murata, Y. H_2O/Olefinic-π Interaction inside a Carbon Nanocage. *J. Am. Chem. Soc.* **2019**, *141*, 12928−12938.

https://doi.org/10.1021/acsphyschemau.3c00068
ACS Phys. Chem Au 2024, 4, 143−147